Continuum numerical modeling of rarefied flows with slip-wall boundary conditions

By S. S. Jain, E. Song†, H. Hwang AND P. Moin

1. Motivation and objectives

Rarefied gas flows are encountered in low-pressure environments such as in high-flying aircraft, re-entry of space vehicles, and dynamics of Earth satellites, and also at standard pressure conditions in microfluidics and microelectromechanical systems. One such application is the manufacturing process of layers of organic light-emitting diodes (OLEDs). In the production process, organic molecules pass through a series of pipes between the chambers as well as nozzles, which causes a severe pressure drop due to an abrupt change in the cross-section of the flow, before they are deposited on to a substrate. Maintaining the uniformity of the thickness of the OLED layers is crucial for the production process, and this requires an accurate control of the system.

The pressure of the OLED production process ranges from 0.1 Pa down to 10^{-5} Pa. At such low pressures, the flow becomes rarefied and can no longer be considered a continuum. The classical continuum methods break down for rarefied gas flows and non-equilibrium effects need to be included, which pose severe challenges in both experiments and numerical simulations of these flows. The traditional Navier–Stokes equations with a no-slip boundary condition becomes inaccurate and underpredicts the mass flow rate (Maurer *et al.* 2003; Ewart *et al.* 2007). The behavior of a rarefied gas flow is accurately described by the Boltzmann equation (Sone 2002). However, solving the Boltzmann equation is computationally challenging due to the cost and the complicated structure of the molecular collision term (Dongari & Agrawal 2012). Therefore, the objectives of this study are to perform numerical simulations of rarefied flow using the traditional Navier-Stokes equations and to assess the accuracy of slip boundary conditions in accounting for the non-equilibrium effects in the rarefied regime.

2. Methods

2.1. *Regimes of rarefied flow*

Rarefied gas flows are characterized by high Knudsen numbers (Kn). Kn is defined as the ratio of the mean free path, λ, to the characteristic length scale of the flow system, l, which serves as a parameter distinguishing different flow regimes: the slip regime $10^{-3} < Kn < 10^{-1}$, the transition regime $10^{-1} < Kn < 10$ and the free-molecular regime $Kn > 10$ (Chambre & Schaaf 2017). The theories of the free-molecular regime and the transition regime are relatively well-developed, while the transition regime requires better understanding and is, therefore, the focus of this study.

The conventional no–slip boundary condition at the solid–fluid interface is applied to flows in the continuum limit ($Kn \ll 1$). For high-Kn flows, however, the velocity slip is proportional to the mean free path. Thus, for rarefied gas flows, it is questionable to

† Samsung Display Co. Ltd., Korea

apply no-slip boundary condition at the wall. A variety of models exist in the literature to address this problem.

Maxwell (1879) derived the first-order slip model. This model in the most general form (assuming isothermal conditions) can be written as

$$\vec{u}_{slip} = \left(\frac{2-\alpha}{\alpha\mu}\right)\lambda\vec{\tau}_t, \tag{2.1}$$

where $\vec{\tau}_t$ is the tangential shear stress and α is the tangential momentum accommodation coefficient. For fully developed flows with planar walls, when used with the Navier-Stokes equations with a linear stress-strain constitutive relationship, this model reduces to the form

$$\vec{u}_{slip} = A_1\lambda\frac{\partial u}{\partial y}, \tag{2.2}$$

where $A_1 = 2 - \alpha/\alpha$. However, the first-order model is valid only for infinitesimally small Mach and Reynolds numbers and up to $Kn \approx 1$. This first-order model also fails to predict the Knudsen minimum—a minimum in the normalized mass flow rate around $Kn \approx 1$—that is observed in experiments (Cercignani & Daneri 1963).

To overcome the shortcomings of the first-order model, many higher-order models have been proposed in the literature (Cercignani & Daneri 1963; Hsia & Domoto 1983; Hadjiconstantinou 2003). The general form of the second-order slip model can be written as

$$\vec{u}_{slip} = A_1\lambda\frac{\partial u}{\partial y} - A_2\lambda^2\frac{\partial^2 u}{\partial y^2}, \tag{2.3}$$

where A_2 is the empirical coefficient for the second-order term. In wall-dominated flows, typical of microfluidic applications, the accuracy of the overall solution is greatly dependent on the accuracy of the boundary condition. This is used as a justification for using a higher-order boundary condition while still using a first-order stress-strain relation (Navier-Stokes equations) for the bulk of the flow (Lockerby *et al.* 2004).

The discrete system of Navier-Stokes equations when used along with the second-order slip model results in an ill-posed system. Lockerby *et al.* (2004) showed that the second-order model can be considered a simplification of the Maxwell slip model when the tangential stress is written in terms of higher-order stress terms. Therefore, it is advisable to use the second-order slip models along with the Burnett equations that have higher-order stress terms. But the Burnett equations are numerically challenging and expensive to solve. This has motivated researchers to use higher-order slip boundary conditions with Navier-Stokes equations, assuming that the improvement in the accuracy of the boundary condition is sufficient to capture the overall accuracy of the solution.

Alternatively, Dufresne (1996) suggested that the pressure gradient in the Knudsen layer is important to capture the characteristics of the flow. Therefore, the first-order slip model can be modified to include pressure gradient effects, to improve the accuracy of the solution. In this study, we refer to this model as the first-order model with pressure compensation. The first-order slip boundary condition along with the pressure gradient term can be written as

$$\vec{u}_{slip} = A_1\lambda\frac{\partial u}{\partial y} - A_3\frac{\lambda}{\alpha\rho c}\frac{\partial p}{\partial x}, \tag{2.4}$$

where A_3 is the empirical coefficient for the pressure gradient term and c is the speed of sound.

Beskok & Karniadakis (1999) developed an empirical model and illustrated that it

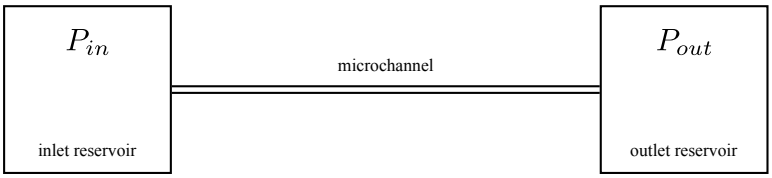

FIGURE 1. Microchannel geometry.

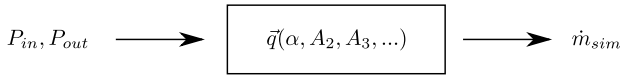

FIGURE 2. Pictorial representation of the system of equations being solved.

works for a wide range of Kn. Nonetheless, this model has constants that needs to be determined by experimental observations or molecular simulation data. The performance of the models on complex geometries also needs to be validated with special care. Thus, this model is not used in this work.

The coefficients that involve tangential momentum accommodation coefficient (α) are nondeterministic; thus, fitting on to the experimental data is unavoidable. Several experiments suggest that various factors affect these coefficients. Agrawal & Prabhu (2008) review several experimental techniques to determine the value of α, nature of the gas, pressure of the gas, surface material, surface cleanliness, surface temperature, gas-solid pair, surface roughness, and curvature. Thus, a procedure to compute deterministic coefficients based on these parameters is desired.

2.2. *Geometry and simulation setup*

In this study, the full implicit solver in the COMSOL software package is used for numerical simulations. The first-order slip, second-order slip, and first-order slip with pressure compensation boundary conditions are implemented in this software package. For the purpose of evaluating the models, we use a rectangular channel geometry from Ewart *et al.* (2007), shown in Figure 1. The dimensions of the channel are length $L = 9.39$ mm, height $H = 9.38$ μm, and width 492 μm. Because the channel length is much longer than its height, the end effects of the channel can be neglected. There are reservoirs on both ends of the channel, which are used in the experiments to maintain a constant pressure at the ends of the channel and to reduce the end effects. We use the reservoirs in the simulation to mimic the experimental setup as closely as possible.

Pressures at the entrance, P_{in}, and exit, P_{out}, of the channel are maintained at constant values, and the mass flow rate at the final steady state is calculated from the simulation. We use the tabulated pressure values in the paper by Ewart *et al.* (2007), and these values approximately correspond to the range of Kn from 0.05 to 50. We then compare the mass flow rate from the simulations with the experimental values.

2.3. *Determination of coefficients*

The system of equations along with the boundary conditions can be written in a concise form as $\vec{q}$, as shown in Figure 2. Here, P_{in} and P_{out}, which represent the inlet and outlet pressures, respectively, are the inputs; $\dot{m}_{sim}$, which represents the computed mass flow rate, is the output; α, A_2, and A_3 are the parameters of the system.

Each pair of P_{in} and P_{out} results in $\dot{m}_{sim}$, and the error in the mass flow rate can be calculated as $E = |\dot{m}_{sim} - \dot{m}_{exp}|$, where $\dot{m}_{exp}$ represents the experimental mass flow rate for a given P_{in} and P_{out}. Thus, if a second-order slip model is used, we have two

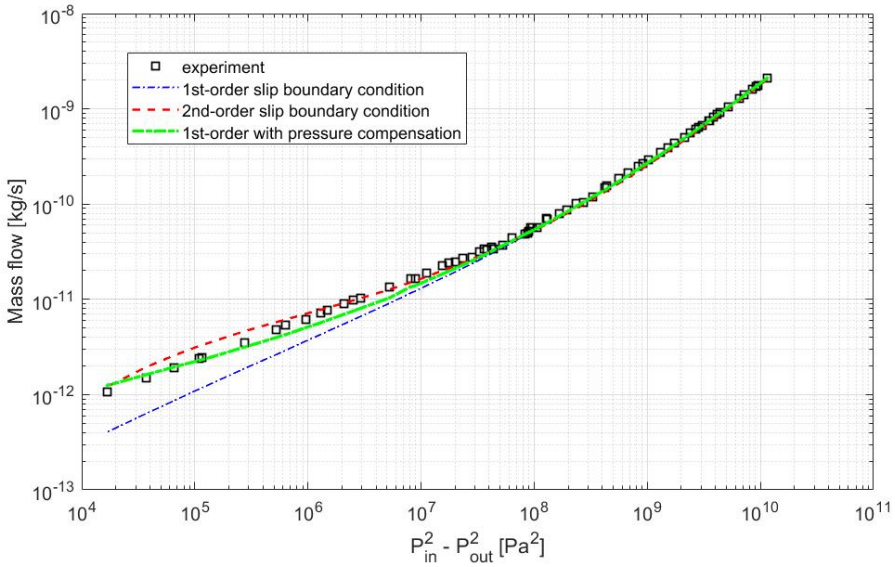

FIGURE 3. Mass flow rate for various P_{in} and P_{out} values and comparison of the numerical simulations with no-slip, first-order slip, second-order slip, and first-order slip with pressure compensation boundary conditions against the experimental data.

unknown coefficients, α and A_2, that are to be determined, but each pair of P_{in} and P_{out} gives a non-zero error E. Therefore, the system is overdetermined. To solve this problem, we set up a non-linear least-square problem that minimizes the sum of E from all the pairs of P_{in} and P_{out}.

3. Results

In this section, we first compute the coefficients in the first-order slip model [Eq. (2.2)], second-order slip model [Eq. (2.3)], and the first-order slip model with pressure compensation [Eq. (2.4)], to simulate rarefied flow with the Navier-Stokes equations, using the procedure described in Section 2.3. We then evaluate the models by comparing the mass flow rate, computed at various Kn, to experimental observations. Most previous studies in microfluidic applications that tried to evaluate or determine the coefficients in the slip models were theoretical. Typically, the mass flow rate is computed in simple geometries along with various simplifications and assumptions, such as a fully developed flow which is not always satisfied, and then compared with the experimental results. Our goal here is to use numerical simulations to solve the Navier-Stokes equations fully when coupled to the slip models to correctly capture the behavior of the flow and determine the coefficients that can be used for the simulation of the full crucible geometry.

We use the least-square minimization procedure described in Section 2.3 to separately compute the coefficients for first-order slip and second-order slip boundary conditions. The results from this procedure yielded values of $\alpha = 0.943$ and $A_2 = 0.195$. The computed mass flow rate is plotted for various P_{in} and P_{out} values and compared against the experiments in Figure 3. There is a clear improvement in the mass flow rate calculation with first-order boundary condition compared with the no-slip boundary condition. The use of the second-order boundary condition also results in improvement compared

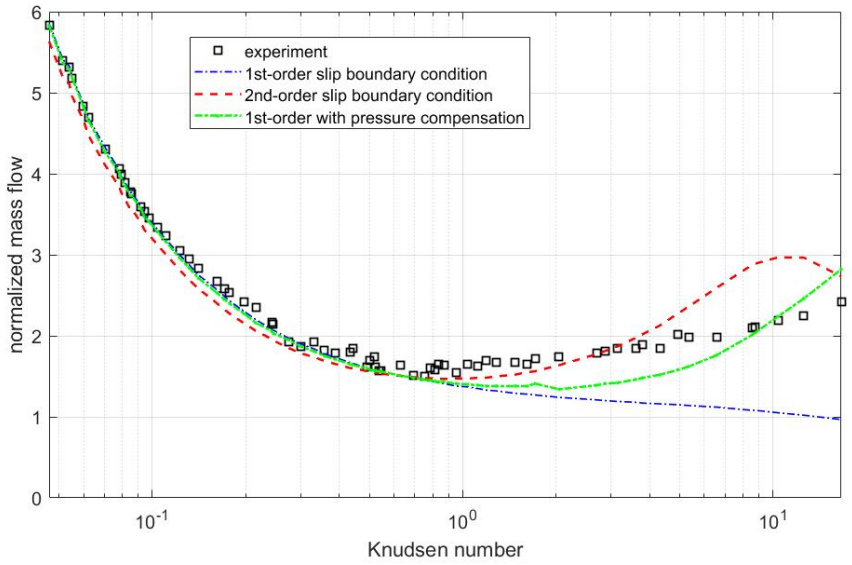

FIGURE 4. Normalized mass flow rate for various Kn values and comparison of the numerical simulations with first-order slip, second-order slip, and first-order slip with pressure compensation boundary conditions against the experimental data.

with the first-order boundary condition. But because the system is ill-posed with the second-order boundary condition, we instead choose to include the effect of the pressure gradient in the first-order slip boundary condition to improve the accuracy of the simulation, as in Eq. (2.4). Following the same least-square minimization procedure above for this boundary condition, the coefficient was found to be $A_3 = 0.1$. Results are shown in Figure 3.

When the normalized mass flow rate is plotted against Kn, a minimum is observed in the mass flow rate at around $Kn \approx 1$, which is referred to as the Knudsen minimum. It is generally known in the literature that the first-order slip model does not capture this Knudsen minimum, which was the motivation to use higher-order slip models. We observe the same behavior with the first-order slip model, as shown in Figure 4. However, the first-order slip model with pressure compensation recovers the Knudsen minimum and, therefore, seems promising.

4. Conclusions

In this work, we evaluated slip boundary conditions for simulating rarefied flow in a microchannel with Navier-Stokes equations. The first-order slip boundary condition improves the mass flow rate compared with the no-slip boundary condition, but does not predict the Knudsen minimum. The second-order boundary condition captures this Knudsen minimum, but this boundary condition when coupled to the Navier-Stokes equations results in an ill-posed system. Therefore, we explore the inclusion of a pressure gradient in the slip boundary condition and show that this results in an improved mass flow rate prediction while maintaining the well-posedness of the system. Additionally, this boundary condition recovers the Knudsen minimum behavior. Work is underway on a microtube geometry to test the accuracy of the slip models in a different geometry.

Acknowledgments

This investigation was funded by Samsung Display Co. Ltd., Korea.

REFERENCES

Agrawal, A. & Prabhu, S. V. 2008 Survey on measurement of tangential momentum accommodation coefficient. *J. Vac. Sci.* **26**, 634–645.

Beskok, A. & Karniadakis, G. E. 1999 Report: a model for flows in channels, pipes, and ducts at micro and nano scales. *Microscale Therm. Eng.* **3**, 43–77.

Cercignani, C. & Daneri, A. 1963 Flow of a rarefied gas between two parallel plates. *J. Appl. Phys.* **34**, 3509–3513.

Chambre, P. A. & Schaaf, S. A. 2017 *Flow of Rarefied Gases*. Princeton University Press.

Dongari, N. & Agrawal, A. 2012 Modeling of Navier–Stokes equations for high Knudsen number gas flows. *Int. J. Heat Mass Transf.* **55**, 4352–4358.

Dufresne, M. A. 1996 *On The Development of a Reynolds Equation for Air Bearings with Contact*. Ph.D. Thesis, Carnegie Mellon University.

Ewart, T., Perrier, P., Graur, I. A. & Méolans, J. G. 2007 Mass flow rate measurements in a microchannel, from hydrodynamic to near free molecular regimes. *J. Fluid Mech.* **584**, 337–356.

Farber, K, Farber, P., Gräbel, J., Krick, S., Reitz, J & Ueberholz, P. 2016 Development and validation of a coupled Navier–Stokes/DSMC simulation for rarefied gas flow in the production process for OLEDs. *Appl. Math. Comput.* **272**, 648–656.

Hadjiconstantinou, N. G. 2003 Comment on Cercignani's second-order slip coefficient. *Phys. Fluids* **15**, 2352–2354.

Hsia, Y-T. & Domoto, G. A. 1983 An experimental investigation of molecular rarefaction effects in gas lubricated bearings at ultra-low clearances. *J. Lubr. Technol.* **105**, 120–129.

Lockerby, D. A., Reese, J. M., Emerson, D. R. & Barber, R. W. 2004 Velocity boundary condition at solid walls in rarefied gas calculations. *Phys. Rev. E* **70**, 017303.

Maurer, J., Tabeling, P., Joseph, P. & Willaime, H. 2003 Second-order slip laws in microchannels for helium and nitrogen. *Phys. Fluids* **15**, 2613–2621.

Maxwell, J. C. 1879 VII. On stresses in rarified gases arising from inequalities of temperature. *Philos. Trans. R. Soc.* **170**, 231–256.

Sone, Y. 2002 *Kinetic Theory and Fluid Dynamics*. Springer.